A NEAR-FIELD APPROACH TO THE SONIC BOOM PROBLEM

By F. A. Woodward

Distribution of this report is provided in the interest of information exchange. Responsibility for the contents resides in the author or organization that prepared it.

D6-15046

August 1967

Prepared under Contract No. NAS 2-3719 by
The Boeing Company
Commercial Airplane Division
P.O. Box 707
Renton, Washington

for

Ames Research Center

NATIONAL AERONAUTICS AND SPACE ADMINISTRATION

CONTENTS

A NEAR-FIELD APPROACH TO THE SONIC BOOM PROBLEM

By F. A. Woodward
The Boeing Company

SUMMARY

Results are presented of an investigation of the feasibility of extending an existing supersonic wing-body analysis and design method (reference 1) to the problem of calculating the pressure signature and associated shock wave pattern in the field surrounding arbitrary airplane configurations at supersonic speed. The conclusion reached is that theoretical methods are presently available to make this extension possible; the steps involved are outlined in some detail.

The principal difference between the above method and the currently accepted theory of Whitham (reference 2) is shown to be in the singularity representations used. The wing-body method represents the configuration by a spatial distribution of singularities over the entire wing and body surfaces, while Whitham's method uses an equivalent linear distribution of singularities along the body axis. In the far field, both methods give the same results, but in the near field, the spatial singularity representation is expected to be superior. An improved understanding of the wave pattern in the near field could lead to new techniques for modifying or reducing the pressure signature in the far field.

INTRODUCTION

Calculations of the pressure signature and shock wave pattern in the field surrounding arbitrary airplane configurations at supersonic speed have been based almost exclusively on a theory presented by G. B. Whitham (reference 2). The predictions of this theory have been verified by extensive wind tunnel and flight test measurements and are generally accepted as a basis for the estimation of sonic boom overpressures.

The present study was undertaken to investigate the feasibility of applying a recently developed wing-body analysis method (reference 1) to the problem of calculating the pressure signature in the near field.[*] In this method, the configuration is represented by a spatial distribution of singularities located in the plane of the wing and along the body axis. Whitham's theory, on the other hand, is based on the slender-body, slender-wing assumption, in which the airplane volume and lift distributions are represented by equivalent line-source distributions located along the body axis only. In the far field, these two distributions of singularities produce flow patterns that become identical asymptotically, but in the near field the spatial distribution of singularities should give superior results. The wave pattern in the near field is of particular importance in sonic boom theory, since it is in this region that the interaction of the waves from the various airplane components occurs. The resulting reinforcement or cancellation of the waves in the near field ultimately determines the level of the far-field pressure signature. Thus, an improved theory in the near field may give additional understanding of the wave interaction problem, which in turn could lead to new techniques for modifying or reducing the pressure signatures in the far field.

The extension of the present wing-body analysis method to calculate the magnitude of the pressures and velocities in the field has already been accomplished. The only additional steps required are to determine the location of the Mach waves in the field to first order, and to insert the shock waves. The techniques involved in accomplishing these steps are outlined in the following

---

[*] In sonic boom theory, the near field is defined as the region between the body and the radial distance at which all the waves generated by the body have coalesced into two distinct shock waves or an N wave pattern. The far field includes all space beyond this radial distance.

paragraphs. The general approach follows that proposed by Whitham very closely, and in fact, is shown to give exactly the same asymptotic result in the far field.

Valuable assistance in the evaluation of some of the integrals tabulated in appendix II was provided by Dr. Tse Sun Chow, a mathematics research specialist at Boeing.

This study was undertaken by the Aerodynamics Research Unit of The Boeing Company, Commercial Airplane Division, as part of NASA contract NAS 2-3719 for the Ames Research Center.

SYMBOLS

C_p	pressure coefficient
F	first-order correction function
k	source strength
K	Constant
m	panel leading-edge slope
M	Mach number
N	number of singularities
r	radial coordinate
R	body radius
S	singularity strength
t	nondimensional variable $x/\beta_\infty r$
T	integral function
u	nondimensional perturbation velocity in x direction
U	freestream velocity
v	nondimensional perturbation velocity in y direction
w	nondimensional perturbation velocity in z direction
x, y, z	cartesian coordinates
y	origin of first-order singularity (Whitham's notation)
α	flow inclination angle
β	$\sqrt{M^2 - 1}$
γ	ratio of specific heats for air
δ	cone half angle
Λ	panel leading-edge sweepback
μ	Mach angle
θ	cylindrical coordinate

Subscripts:

∞	freestream condition
j	singularity number
r	radial direction
s	source, shock wave
v	vortex
θ	theta direction
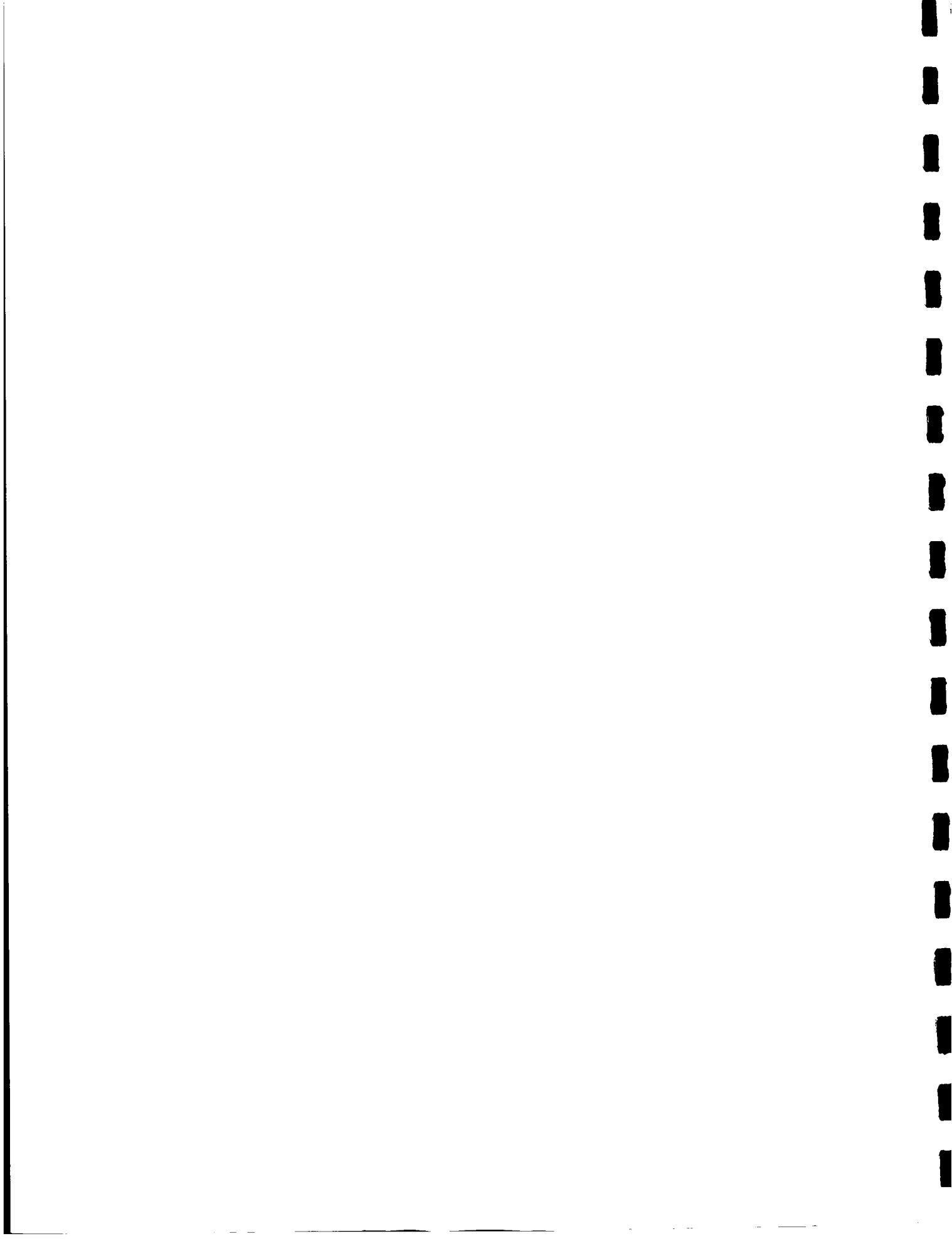
AERODYNAMIC THEORY

Perturbation velocity components u, v, and w at any point P (x, y, z) in the field surrounding an arbitrary wing-body combination in supersonic flow may be calculated to first order by the method of singularities (reference 1). At the present stage of development, the singularities are located along the body axis and on panels distributed over the wing and body surfaces. Singularity strengths are determined by boundary conditions specified at control points on the surface and govern the magnitude of velocity components in the field.

In the following discussion, the contribution of an individual singularity is considered. The flow-field disturbance created by an individual singularity is conical and bounded by a Mach cone having its apex at the origin of the singularity. However, it should be emphasized that the net disturbance in the flow-field surrounding this singularity is that due to the sum of the contributions of all the singularities used to represent the configuration. Therefore, the disturbance field created by the wing-body combination is bounded by an envelope of the Mach cones originating from each of the singularities used in the representation, which may not be conical. In linearized theory, the flow field within this envelope of Mach cones is referred to as a zero-order flow field since the disturbances are assumed to propagate into the field at the speed of sound of the fluid at rest. The slope at an outgoing Mach wave of the zero-order flow field is given by

$$\frac{dx}{dr} = \cot \mu_\infty = \sqrt{M_\infty^2 - 1} = \beta_\infty \tag{1}$$

where μ_∞ is the Mach angle of the undisturbed flow.

Whitham's theory for determining the flow pattern assumes that the linearized theory of supersonic flow gives a valid first approximation to the magnitude of the velocity components everywhere in the field, provided that the approximate characteristics of the Mach cone envelope are replaced by a sufficiently good approximation to the exact characteristics. The slope of the exact characteristic of an outgoing wave is given by

$$\frac{dx}{dr} = \cot (\mu + \alpha) = \frac{\cot \mu - \tan \alpha}{1 + \cot \mu \tan \alpha} \tag{2}$$

where μ is the local Mach angle based on the local Mach number M, and α is the local inclination of the stream measured from the freestream direction. Place

$$\cot \mu = \beta = \sqrt{M^2 - 1}$$

$$\tan \alpha = v_r$$

where v_r is the ratio of the velocity in the radial direction to the freestream velocity U_∞. Then for small values of βv_r, equation (2) may be written approximately

$$\frac{dx}{dr} \approx \beta - M^2 v_r \tag{3}$$

For large values of βv_r, equation (3) cannot be expanded in this manner to obtain an approximation to the slope of the characteristic. In this case, for small v_r, equation (2) may be inverted and expanded as follows:

$$\frac{dr}{dx} \approx \frac{1}{\beta} + \frac{M^2}{\beta^2} v_r \tag{4}$$

Equation (4) gives a more accurate estimate of the slope of the characteristic for high Mach numbers. Equations (3) and (4) may be put into their final forms by introducing a linear relationship between the local Mach number and pressure coefficient. The relationship used is compared with the exact isentropic relationship in figure 1. If, in addition, the linear theory pressure coefficient relationship $C_p = -2u$ is assumed, then

$$M \approx M_\infty \left[1 + (1 + \frac{\gamma - 1}{2} M_\infty^2) u \right]$$

$$\beta = \sqrt{M^2 - 1} \approx \beta_\infty + \frac{M_\infty^2}{\beta_\infty}(1 + \frac{\gamma - 1}{2} M_\infty^2) u \tag{5}$$

giving

$$\frac{dx}{dr} \approx \beta_\infty + \frac{\gamma + 1}{2} \frac{M_\infty^4}{\beta_\infty} u - M_\infty^2 (v_r + \beta_\infty u) \tag{6}$$

for low Mach numbers and

$$\frac{dr}{dx} \approx \frac{1}{\beta_\infty} - \frac{\gamma + 1}{2} \frac{M_\infty^4}{\beta_\infty^3} u + \frac{M_\infty^2}{\beta_\infty^2} (v_r + \beta_\infty u) \tag{7}$$
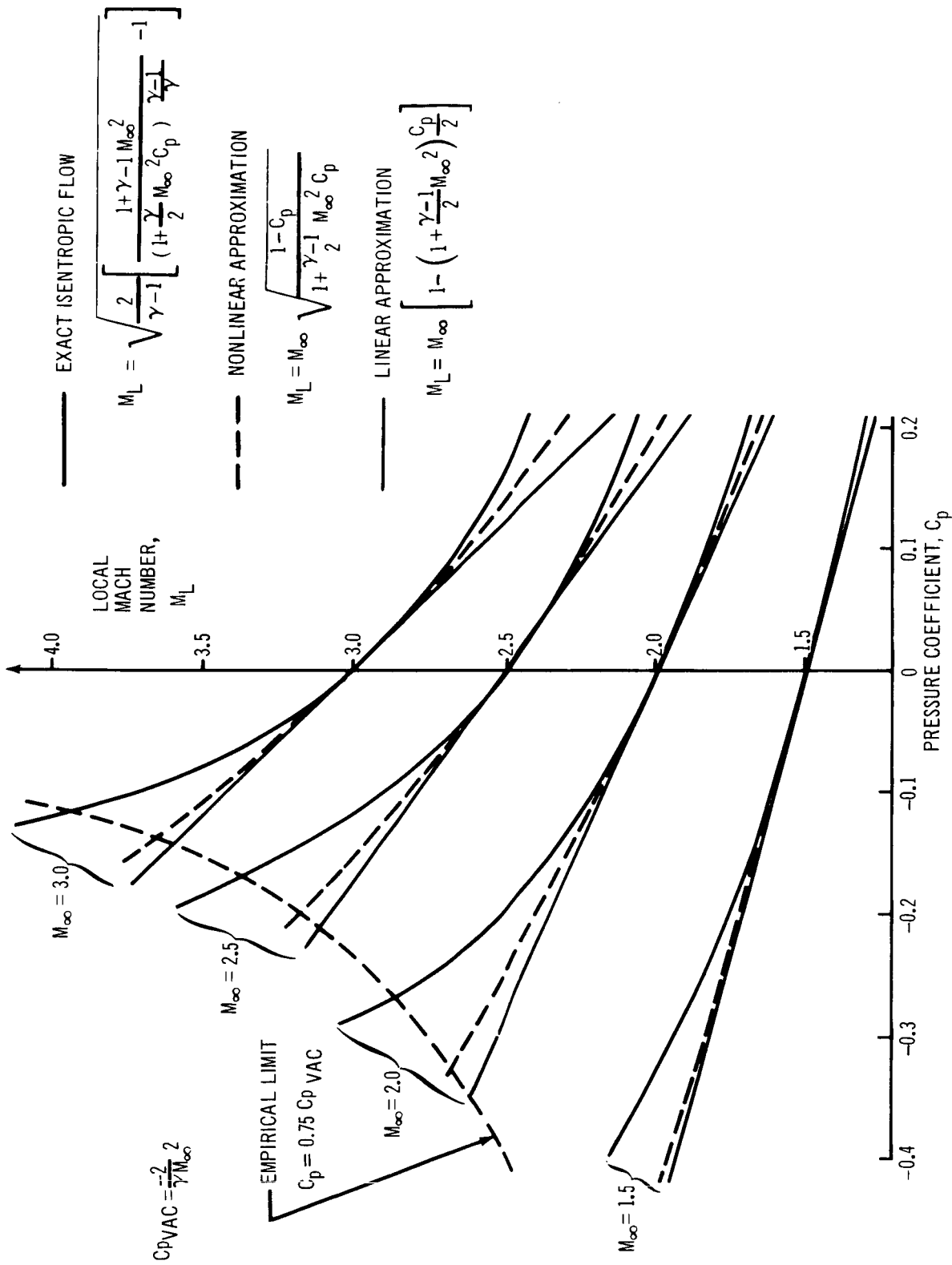
for high Mach numbers.

EXACT ISENTROPIC FLOW

$$M_L = \sqrt{\frac{2}{\gamma-1}\left[\frac{1+\gamma-1\,M_\infty^2}{\left(1+\frac{\gamma-1}{2}M_\infty^2 C_p\right)^{\frac{\gamma-1}{\gamma}}} - 1\right]}$$

NONLINEAR APPROXIMATION

$$M_L = M_\infty \sqrt{\frac{1-C_p}{1+\frac{\gamma-1}{2}M_\infty^2 C_p}}$$

LINEAR APPROXIMATION

$$M_L = M_\infty \left[1-\left(1+\frac{\gamma-1}{2}M_\infty^2\right)\frac{C_p}{2}\right]$$

LOCAL MACH NUMBER, M_L

4.0

3.5

3.0

2.5

2.0

1.5

$M_\infty = 3.0$

$M_\infty = 2.5$

$C_{p\,VAC} = \frac{-2}{\gamma M_\infty^2}$

EMPIRICAL LIMIT
$C_p = 0.75\ C_p\ VAC$

$M_\infty = 2.0$

$M_\infty = 1.5$

PRESSURE COEFFICIENT, C_p

-0.4   -0.3   -0.2   -0.1   0   0.1   0.2

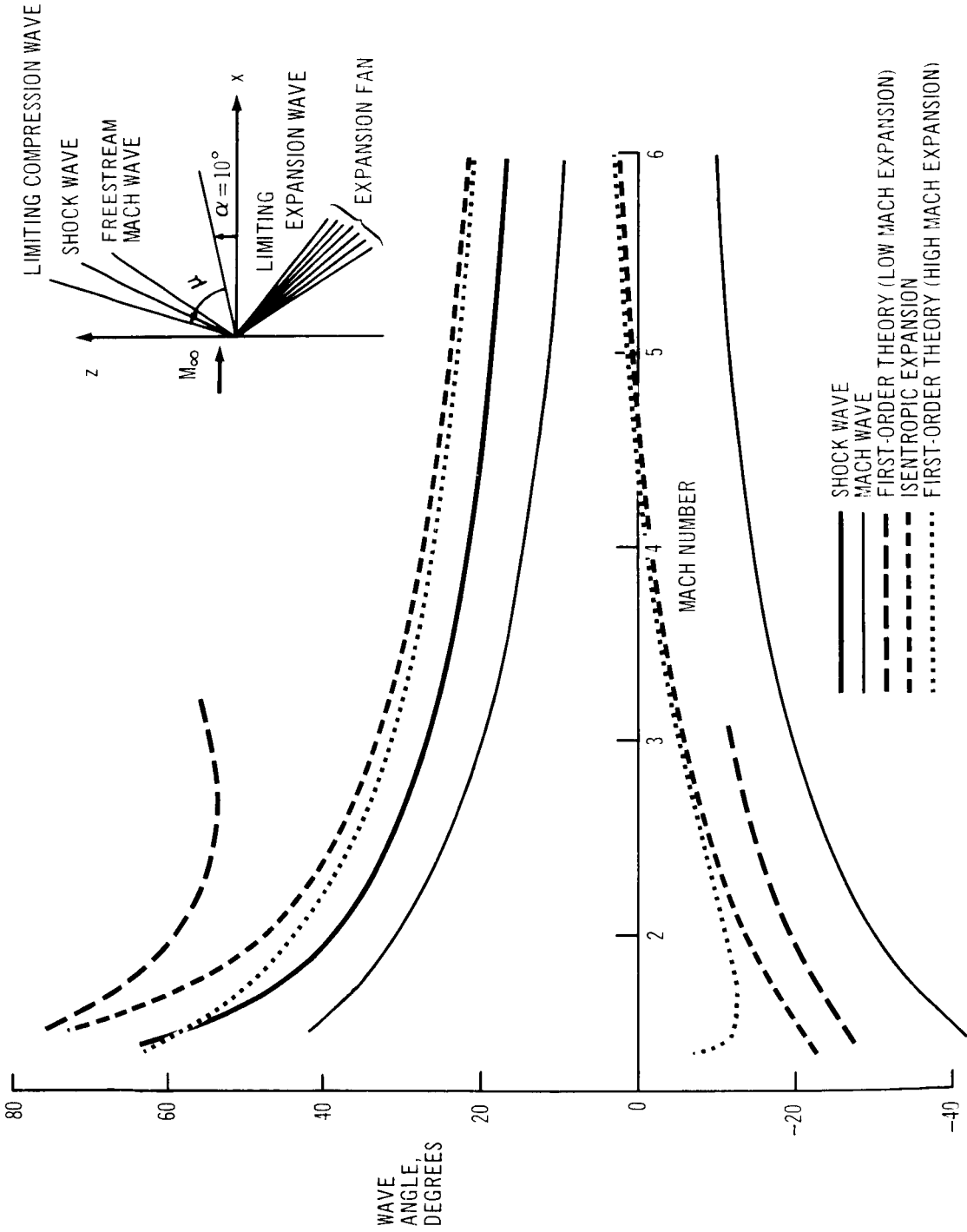*Figure 1. Mach Number and Pressure Coefficient Approximations*

9

Figure 2. Flat Plate Wave Inclination

10

The range of validity for each of these approximate formulas is illustrated on figure 2, which shows the wave pattern in the flow around an unswept plate at 10 degrees incidence. In the figure, the wave angle $\mu + \alpha$ measured from the freestream direction is plotted as a function of Mach number for both the compression and expansion sides of the plate. The Mach wave angle μ_∞ of the undisturbed flow is shown on both sides for reference. In addition, the angle of the limiting isentropic expansion wave of a Prandtl-Meyer fan is shown for the expansion side, and the shock wave and limiting isentropic compression wave angles are shown for the compression side. The range of validity of equation (6) is seen to be quite small in this example, while equation (7) gives a good approximation for all Mach numbers greater than 2. It should be noted that Whitham's theory uses equation (6) to approximate the characteristic direction of the outgoing waves and, as a result, may introduce significant errors if the theory is applied at high Mach numbers. In this study, both equations (6) and (7) have been used to approximate the slope of the outgoing Mach waves and the results of each calculation compared.

Equations of First-Order Mach Waves

Equations (6) and (7) give alternate expressions for the slope of an outgoing Mach wave in terms of the velocity components along it. The equation of the trace of the wave in a plane θ = constant may be obtained by substituting the appropriate expressions for u and v_r into these equations and integrating.

For low Mach numbers, the velocity components at a point P (x, r, θ) lying on the first-order Mach wave from a point Q $(x_0 + \beta_\infty R, R, \theta)$ on the body surface are assumed to be equal to those evaluated by linearized theory at a point P' $(x + \Delta x, r, \theta)$ lying on the zero-order Mach wave passing through Q. The zero-order Mach wave intercepts the body axis at $x = x_0$. This is equivalent to assuming that the first-order Mach forecone from P intercepts the same number of singularities on the body axis as the zero-order Mach forecone from P'. The geometry is illustrated at the top of the next page.
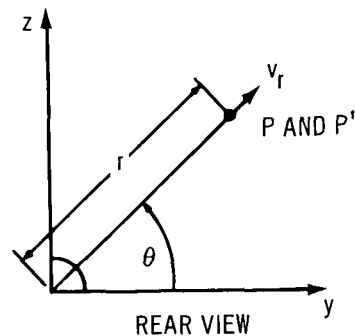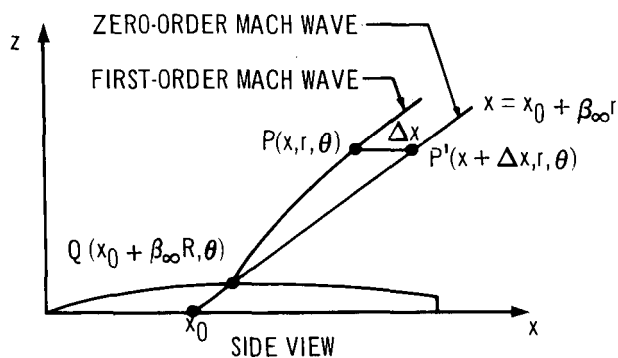Since

$$x + \Delta x = x_0 + \beta_\infty r$$

then

$$u(x, r, \theta) = u(x_0 + \beta_\infty r, r, \theta)$$

$$v_r(x, r, \theta) = v_r(x_0 + \beta_\infty r, r, \theta)$$

(8)

ZERO-ORDER MACH WAVE
FIRST-ORDER MACH WAVE
$x = x_0 + \beta_\infty r$
$P(x, r, \theta)$
Δx
$P'(x + \Delta x, r, \theta)$
$Q(x_0 + \beta_\infty R, \theta)$
x_0
SIDE VIEW
x
z

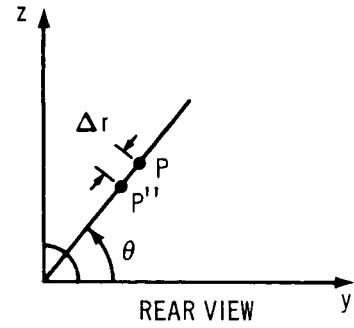REAR VIEW
z
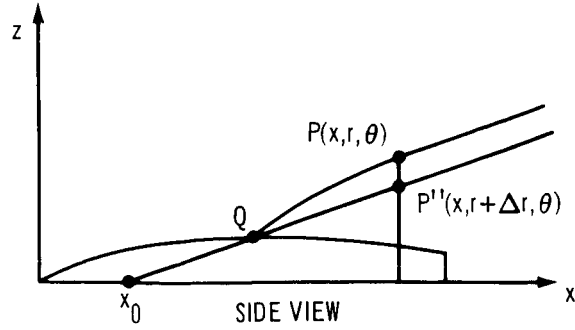v_r
P AND P'
r
θ
y

Substituting these expressions into equation (6) and integrating with respect to r, an equation for the first-order Mach line in the plane θ = constant is obtained.

$$
x = x_0 + \beta_\infty r + \frac{\gamma + 1}{2} \frac{M_\infty^4}{\beta_\infty} \int_R^r u(x_0 + \beta_\infty r, r, \theta) \, dr
$$

$$
- M_\infty^2 \int_R^r \left[v_r(x_0 + \beta_\infty r, r, \theta) - \beta_\infty u(x_0 + \beta_\infty r, r, \theta) \right] dr
$$

(9)

where x_0 is the value of x for r = 0, and R is the value of r where the Mach line emerges from the surface of the body. It should be noted that the wave distortion Δx is given by the sum of the two integrals in equation (9). The evaluation of these integrals will be discussed in the next section.

For high Mach numbers, a slightly different assumption must be made for the values of the velocity components at P. In this case, the Mach waves lie much closer to the body surface, so it is assumed that the velocity components there are equal to those evaluated by linearized theory at a point $P''(x, r + \Delta r, \theta)$. P'' lies on the zero-order Mach cone that passes through Q and intercepts the body axis at x_0. The geometry of this case is illustrated at the top of the next page.

SIDE VIEW

REAR VIEW

Now

$$r + \Delta r = \frac{x - x_0}{\beta_\infty}$$

so

$$u(x, \ r, \ \theta) = u\left(x, \frac{x - x_0}{\beta_\infty}, \ \theta\right)$$

$$v_r(x, \ r, \ \theta) = v_r\left(x, \frac{x - x_0}{\beta_\infty}, \ \theta\right)$$

(10)

Substituting these expressions into equation (7) and integrating with respect to x, an alternate equation for the first-order Mach line in the plane θ = constant is obtained.

$$r = \frac{x - x_0}{\beta_\infty} - \frac{\gamma + 1}{2} \frac{M_\infty^4}{\beta_\infty^3} \int_{x_0 + \beta_\infty r}^{x} u\left(x, \frac{x - x_0}{\beta_\infty}, \ \theta\right) dx$$

$$+ \frac{M_\infty^2}{\beta_\infty^2} \int_{x_0 + \beta_\infty R}^{x} \left[v_r\left(x, \frac{x - x_0}{\beta_\infty}, \ \theta\right) + \beta_\infty u\left(x, \frac{x - x_0}{\beta_\infty}, \ \theta\right)\right] dx$$

(11)

Again, the wave distortion Δr is given by the sum of the two integrals in equation (11). In equations (9) and (11),

$$v_r = v \cos \theta + w \sin \theta$$

when v and w are given in cartesian coordinates.

13

Classification of Velocity Components

The wing-body combination may be represented by as many as seven different types of singularities, as indicated on figure 3. The body is represented by a combination of line sources and doublets, the wing thickness by planar source distributions, and the wing lift and interference effects by planar vortex distributions. The seven elementary singularities used in the representation are listed below:

1. Linear source
2. Quadratic source
3. Linear doublet
4. Quadratic doublet

Line singularities

5. Constant source sheet
6. Linear source sheet
7. Constant vortex sheet

Planar singularities

Formulas for the velocity components corresponding to these seven elementary singularity distributions are listed in appendix I. In this list, all coordinates are referred to the origin of the singularity.

The resultant velocity at any point in the disturbance field from a wing-body combination is obtained by summing the products of the elementary velocity components and their respective singularity strengths, for each singularity used in the representation. For example, for a configuration consisting of $N1$ sources and $N2$ vortex singularities,

$$u = \sum_{j=1}^{N1} u_{s_j} S_{s_j} + \sum_{j=1}^{N2} u_{v_j} S_{v_j}$$

$$v = \sum_{j=1}^{N1} v_{s_j} S_{s_j} + \sum_{j=1}^{N2} v_{v_j} S_{v_j} \qquad (12)$$

$$w = \sum_{j=1}^{N1} w_{s_j} S_{s_j} + \sum_{j=1}^{N2} w_{v_j} S_{v_j}$$

where

S_{s_j} is the strength of the jth source

S_{v_j} is the strength of the jth vortex

14

BODY THICKNESS

    1. LINEAR SOURCE
    2. QUADRATIC SOURCE

BODY CAMBER AND INCIDENCE

    3. LINEAR DOUBLET
    4. QUADRATIC DOUBLET

WING THICKNESS

    5. CONSTANT SOURCE SHEET
    6. LINEAR SOURCE SHEET

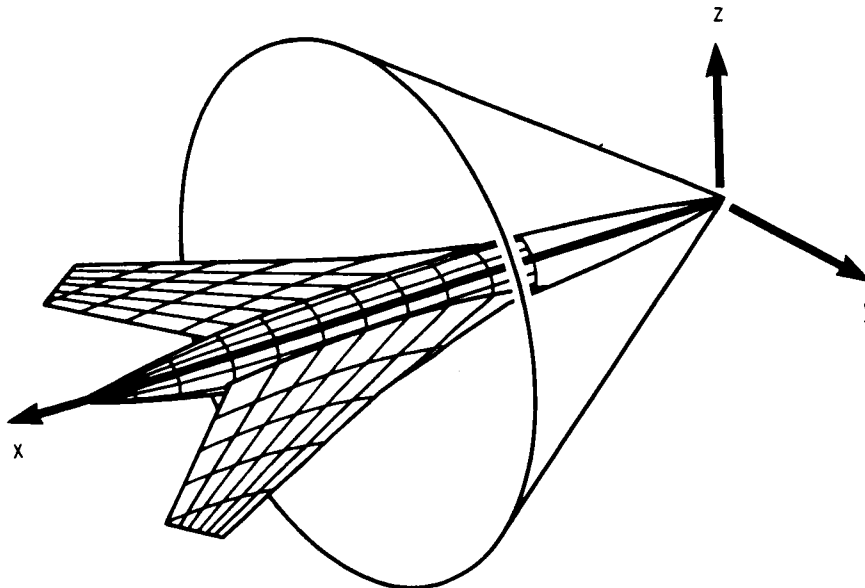WING CAMBER, INCIDENCE, AND WING-BODY INTERFERENCE

    7. CONSTANT VORTEX SHEET

Figure 3. Basic Singularities

15

The integrals appearing in equations (9) and (11) are made up of sums of elementary velocity component expressions of the types listed in appendix I. An examination of this list shows that these expressions are composed of combinations of the nine functions listed below.

$$T_1 = \cosh^{-1} t$$

$$T_2 = \sqrt{t^2 - 1}$$

$$T_3 = \cosh^{-1} \frac{t - \beta_\infty m \cos \theta}{\sqrt{(\beta_\infty mt - \cos t)^2 + (1 - \beta_\infty^2 m^2) \sin^2 \theta}}$$

$$T_4 = \tan^{-1} \frac{\beta_\infty m \sin \theta \sqrt{t^2 - 1}}{1 - \beta_\infty mt \cos \theta}$$

$$T_5 = rT1$$

$$T_6 = rT2$$

$$T_7 = \frac{T2}{r}$$

$$T_8 = rT3$$

$$T_9 = rT4 \tag{13}$$

where

$$t = \frac{x}{\beta_\infty r}, \quad m = \cot \Lambda$$

For use in equation (9), these functions must be integrated with respect to r, with $x = x_0 + \beta_\infty r$. For use in equation (11), they must be integrated with respect to x, with $r = (x - x_0)/\beta_\infty$. In fact, only one integration need be performed in either case, as the variables can be interchanged without changing the form of the functions. These integrals have all been evaluated as part of this study and are listed in appendix II.

For low Mach numbers, equation (9) now gives an explicit expression for the x coordinate of the first-order Mach wave from x_0 in terms of the radius r.

$$x = x_0 + \beta_\infty r + x_0 \left\{ K - M_\infty^2 \sum_{j=1}^{N} \left[\frac{\gamma+1}{2} \frac{M_\infty^2}{\beta_\infty^2} F_{1_j} \left(\frac{\beta_\infty r}{x_0} \right) + F_{2_j} \left(\frac{\beta_\infty r}{x_0} \right) \right] S_j \right\} \tag{14}$$

where

$$F_{1_j} = \int_R^r u_j(x_0 + \beta_\infty r,\ r,\ \theta)\ dr$$

$$F_{2_j} = \int_R^r \left[v_{r_j}(x_0 + \beta_\infty r,\ r,\ \theta) - \beta_\infty u_j(x_0 + \beta_\infty r,\ r,\ \theta) \right] dr$$

$$K = M_\infty^2 \sum_{j=1}^N \left[\frac{\gamma+1}{2} \frac{M_\infty^2}{\beta_\infty^2} F_{1_j}\left(\frac{\beta_\infty R}{x_0}\right) + F_{2_j}\left(\frac{\beta_\infty R}{x_0}\right) \right] S_j$$

For high Mach numbers, equation (11) similarly gives an explicit expression for r as a function of x for given x_0. In nondimensional form,

$$\frac{\beta_\infty r}{x_0} = \frac{x}{x_0} - 1 - \left\{ K - M_\infty^2 \sum_{j=1}^N \left[\frac{\gamma+1}{2} \frac{M_\infty^2}{\beta_\infty^2} F_{1_j}\left(\frac{x}{x_0}\right) + F_{2_j}\left(\frac{x}{x_0}\right) \right] S_j \right\} \tag{15}$$

where

$$F_{1_j} = \int_{x_0 + \beta_\infty R}^x u_j\left(x,\ \frac{x - x_0}{\beta_\infty},\ \theta\right) dx$$

$$F_{2_j} = \int_{x_0 + \beta_\infty R}^x \left[v_{r_j}\left(x,\ \frac{x - x_0}{\beta_\infty},\ \theta\right) - \beta_\infty u_j\left(x,\ \frac{x - x_0}{\beta_\infty},\ \theta\right) \right] dx$$

Depending on the Mach number, either equation (14) or (15) may be used to define the first-order Mach waves.

Relationship to Whitham's Theory

The function $F_1(t)$, where $t = \beta_\infty r/x_0$ in equation (14), or $t = x/x_0$ in equation (15), is related to Whitham's function $F(y)$ where $y \equiv x_0$ in the present notation. This can be demonstrated by considering the flow field about a simple cone of half angle δ. For this example, linearized theory gives

$$u = -k\ \cosh^{-1} \frac{x}{\beta_\infty r}$$

$$v = k\beta_\infty \sqrt{\left(\frac{x}{\beta_\infty r}\right)^2 - 1} \tag{16}$$

where

$$k = \frac{\tan^2 \delta}{\sqrt{1 - \beta_\infty^2 \tan^2 \delta} + \tan^2 \delta \cosh^{-1} \frac{1}{\beta_\infty \tan \delta}}$$

Therefore,

$$F_1(t) = k \left[\sqrt{1 + 2t} + t \cosh^{-1}\left(1 + \frac{1}{t}\right) \right]$$

$$F_2(t) = k \left[\sqrt{1 + 2t} - (1 + t) \cosh^{-1}\left(1 + \frac{1}{t}\right) \right]$$

$$K = \frac{\gamma + 1}{2} \frac{M_\infty^4}{\beta_\infty^2} k \left[\sqrt{\frac{1 + \beta_\infty \tan \delta}{1 - \beta_\infty \tan \delta}} + \frac{\beta_\infty \tan \delta}{1 - \beta_\infty \tan \delta} \cosh^{-1} \frac{1}{\beta_\infty \tan \delta} \right] \tag{17}$$

$$+ M_\infty^2 k \left[\sqrt{\frac{1 + \beta_\infty \tan \delta}{1 - \beta_\infty \tan \delta}} - \frac{1}{1 - \beta_\infty \tan \delta} \cosh^{-1} \frac{1}{\beta_\infty \tan \delta} \right]$$

In the far field, $t \to \infty$.

It is shown in Reference 3 that

$$\lim_{x \to 1} \cosh^{-1} \frac{1}{x} = \sqrt{2(1 - x)}$$

Similarly,

$$\lim_{t \to \infty} t \cosh^{-1} \left(1 + \frac{1}{t}\right) = \sqrt{2t}$$

and

$$F_1(t) \to 2\sqrt{2t}$$

$$F_2(t) \to 0$$

so that the asymptotic form of equations (14) or (15) is

$$x = x_0 + \beta_\infty r - \frac{\gamma + 1}{\sqrt{2}} \frac{M_\infty^4}{\beta_\infty^{3/2}} 2 k \sqrt{r x_0} \tag{18}$$

which is exactly equivalent to Whitham's formula for a cone

$$x = x_0 + \beta_\infty r - \frac{\gamma + 1}{\sqrt{2}} \frac{M_\infty^4}{\beta_\infty^{3/2}} F(y) \sqrt{r} \tag{19}$$

where

$$F(y) = 2\delta^2 \sqrt{y} = 2\delta^2 \sqrt{x_0}$$

provided the cone is sufficiently slender so that $k \equiv \delta^2$. Therefore, equations (14) or (15) give expressions for the Mach line $x_0 = $ constant in the entire flow field. An example showing the curvature of the Mach line near a 15-degree cone at $M_\infty = 3.0$ is presented in figure 4.

Theoretical Comparisons for Cones

The first-order flow field theory is easily illustrated by calculating the flow about a simple cone. Only one singularity is required in this example, but this is sufficient to demonstrate the effect of the high and low Mach number approximations on the shape of the Mach waves, the development of a limit cone, and the resultant distortion of the pressure signature in the field. In addition, the location of the front shock wave can be estimated and compared to that given by the cone tables and that predicted by Whitham's theory.

The first-order Mach waves have been calculated using equations (14) and (15) for a 15-degree cone at $M_\infty = 3.0$. The shape of the resulting Mach lines are shown in figure 4. A considerable difference is observed between these two calculations, with the high Mach number solution of equation (15) appearing to give the most realistic approximation to the first-order Mach lines.

Both solutions show the development of a limit cone, which in this case is an exact cone from the origin just tangent to the envelope of the first-order Mach waves. The limit cone indicates the most forward extent of the disturbance.

The pressure signature corresponding to each solution is also indicated on the figure, for $r = 1/\beta_\infty = 0.354$. The zero-order solution shows a gradual pressure rise from zero at the undisturbed Mach cone at $x = 1.0$ to a value of $C_p = 0.16$ on the surface. The low Mach number approximation predicts a considerable distortion of this pressure signature, which extends forward to just touch the limit cone. The high Mach number approximation gives a more moderate distortion. Each signature returns to the same value on the cone surface.

The forward curvature of the pressure signature between the Mach cone and the limit cone represents a physically unrealistic solution. It is generally assumed that a shock wave will develop in this region, which will introduce a discontinuous pressure rise from zero to some value on the upper limb of the pressure curve. The shock wave location is determined by applying the principal that the slope $(dx/dr)_S$ of the shock wave lies halfway between the slope of the undisturbed Mach wave β_∞ and the first-order Mach wave directly behind it. For a cone, the slope at the shock wave is given by

$$\left(\frac{dx}{dr}\right)_S = \beta_\infty \left\{ 1 - \frac{M_\infty^2 k}{2} \left[\left(\frac{\gamma + 1}{2} \frac{M_\infty^2}{\beta_\infty^2} - 1 \right) \cosh^{-1} \left(1 + \frac{1}{t} \right) + \frac{\sqrt{1 + 2t}}{t} \right] \right\} \quad (20)$$
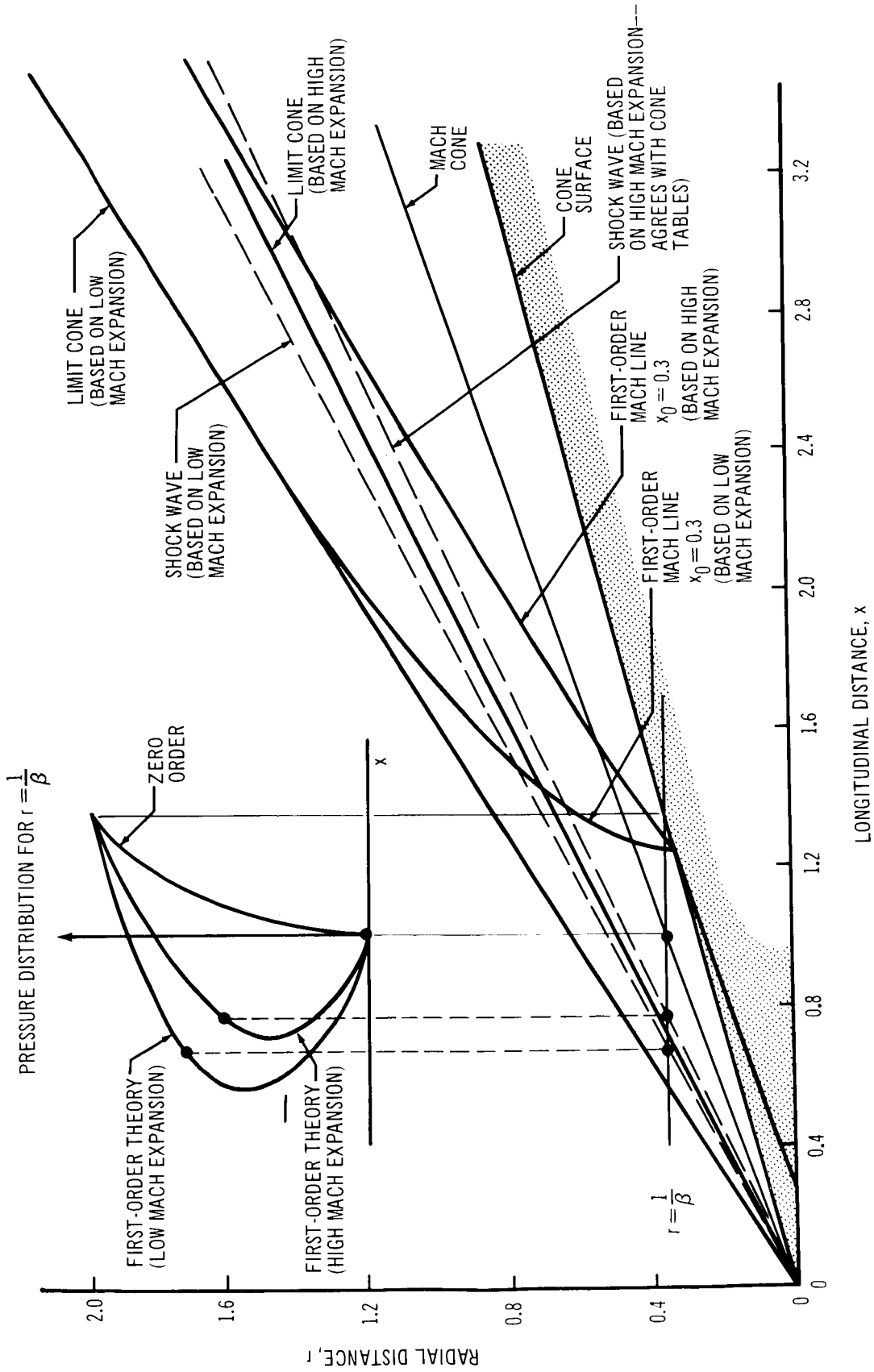
Figure 4. Shock Wave Locations for 15° Cone at Mach 3.0

20

but the slope of the shock wave is also given by

$$\left(\frac{x}{r}\right)_s = \beta_\infty \left\{ 1 + \frac{1}{t}\left[1 + K - M_\infty^2 k \left(\frac{\gamma + 1}{2} \frac{M_\infty^2}{\beta_\infty^2} F_1(t) + F_2(t) \right) \right] \right\} \qquad (21)$$

These two equations may be solved graphically to determine t_s and x_s directly. It is of interest to note that the application of this method to the Whitham theory for cones gives

$$\left(\frac{dx}{dr}\right)_s = \beta_\infty - \frac{3}{8} \frac{(\gamma + 1)^2 M_\infty^8}{\beta_\infty^3} \delta^4 \qquad (22)$$

This is identical to the equation obtained by Whitham by another method.

The position of the shock waves corresponding to both the low Mach number and high Mach number approximations are indicated on the figure and compared with the exact shock wave position obtained from the cone tables. The high Mach number solution gives an accurate estimate of the shock wave location in this example. On the other hand, Whitham's formula, equation (22), gives a completely unrealistic negative result.

A comparison of the first-order limit cone and pressure signature determined from equation (14) with that given by Whitham is presented in figure 5 for a 10-degree cone at $M_\infty = 3.0$. In this example, Whitham's shock wave formula gives a more realistic result but still shows considerable error when compared with the exact result from the cone tables. The present first-order theory gave very close agreement with the exact result in this example, however.

The shock wave locations for both 10- and 15-degree cones have been calculated for three different Mach numbers using equations (20) and (21) and presented in figure 6. Also, shown on the figure are the exact results given by the cone tables, and Whitham's approximation, equation (22). In this calculation, the effect of using the high and low Mach number approximations to the first-order theory (equations (15) and (14), respectively) is also shown. Based on the relatively few calculations done during this study, the low Mach number approximation seems to be adequate for predicting the shock wave location on cones provided the freestream Mach cone is relatively far from the cone surface. For high Mach numbers, the high Mach number approximation is superior for the blunter cones. Whitham's approximate formula is definitely inferior for 15-degree cones at all Mach numbers, and for 10-degree cones above $M_\infty = 2.0$.

The differences between the present first-order theory and Whitham's theory diminish with distance from the body, and the two theories become identical at an infinite distance from the source. However, the relative position of the shock wave from the nose depends on the accuracy to which the flow field is predicted in both the near and far fields.

It is clear that the present method can be expected to give improved pressure signatures in the near field, particularly for bodies having fairly blunt noses at higher Mach numbers. It is also probable that the method will give improved estimates for the location of shock wave coalescence for any configuration and Mach number.
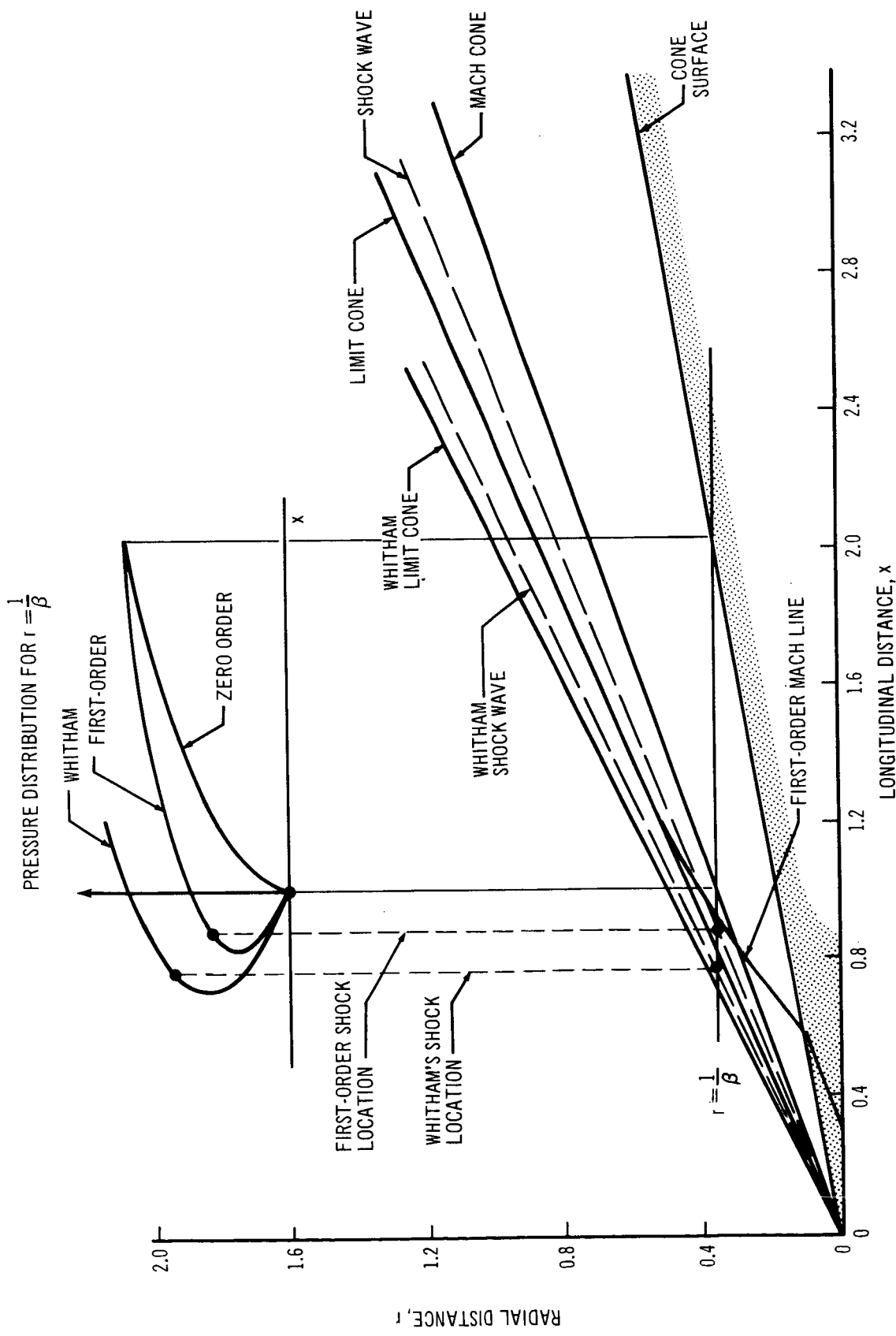
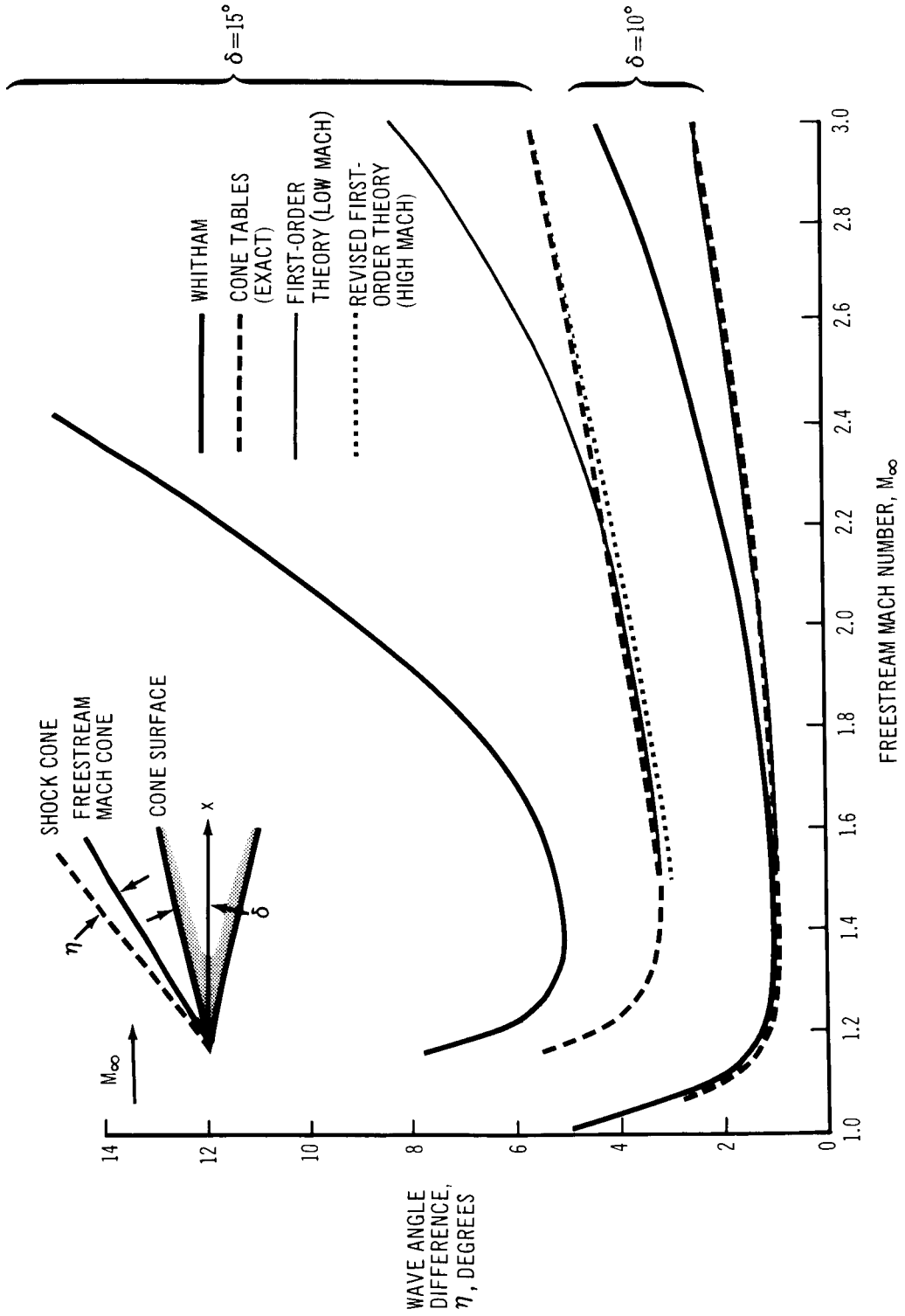Figure 5. Shock Wave Locations for 10° Cone at Mach 3.0

23

Figure 6. Cone Wave Locations

WHITHAM

CONE TABLES (EXACT)

FIRST-ORDER THEORY (LOW MACH)

REVISED FIRST-ORDER THEORY (HIGH MACH)

$\delta = 15°$

$\delta = 10°$

FREESTREAM MACH NUMBER, M_∞

WAVE ANGLE DIFFERENCE, η, DEGREES

SHOCK CONE

FREESTREAM MACH CONE

CONE SURFACE

M_∞

η

δ

x

24

DEVELOPMENT PROCEDURE

The development of this method to calculate the pressure signatures, including shock waves, for arbitrary airplane configurations in both near and far fields appears to be possible at this time. The development would logically proceed along two lines: one would be to extend the existing supersonic wing-body analysis program to include horizontal and vertical tails, canards, and nacelles; the other would be to study the contribution of each of these components to the pressure signature in the field. In addition, a procedure for estimating the shock wave locations in the field would be required. The various aspects of these problems will be discussed in more detail below.

Extension of Wing-Body Program

The extension of the existing wing-body program (reference 1) to include the effects of horizontal and vertical tails, canards, and nacelles would not be a major undertaking. No new types of singularities are required for this extension of the program, only a redistribution of existing types.

If an increase in the total number of singularities is required to give an adequate representation of an arbitrary airplane configuration, the program changes may be more difficult. The present limits of 100 wing panels, 100 body panels, and 50 line sources and doublets have been set to allow matrix inversion without partition within the core of the IBM 7094 computer. An increase in these limits would require fairly extensive reprogramming.

Development of Flow-Field Program

The wing-body program has been extended to calculate the first-order velocities and pressures in the surrounding zero-order flow field under the present contract (NAS 2-3719). Development of this program to calculate the pressure signatures of an arbitrary airplane configuration uniformly to first order would follow the theoretical method outlined in the previous section. The steps necessary to develop this program are given below.

1. The functions $F_1(t)$ and $F_2(t)$ for each of the seven elementary singularities would be formulated in terms of the integrals already evaluated and listed in appendix II.

2. The flow field surrounding an isolated body of revolution would be calculated using the four line singularities. Then the effect of body thickness

distribution, incidence, and camber could be investigated in both the near and far fields, and the far-field result could be compared to Whitham's theory.

3. The flow field surrounding an isolated wing at zero lift would be calculated next using the two planar source singularities. The effect of wing thickness distribution, planform, and subsonic and supersonic edges could be investigated in both the near and far fields. Again, the far-field result should be compared to Whitham's theory.

4. The flow field surrounding an isolated lifting wing would be calculated, with lift effects being represented by the planar vortex singularity. This would permit investigation of planform, subsonic and supersonic edges, camber, and incidence effects for wings with and without thickness in both the near and far fields. As before, the far-field result would be compared to Whitham's theory, while the near-field result could be compared with Lighthill's first-order theory for the field surrounding subsonic leading edge delta wings and rectangular wing tips (reference 3).

5. The flow field surrounding arbitrary wing-body and airplane configurations would be calculated. The effects of wing height on the fuselage, wing thickness and camber, shielded bodies, nacelles, and tails, could be investigated. Development of the configuration pressure signature and coalescence of the shock waves from the wing and body could be studied in detail within the near field and beyond. The far-field result should be compared with Whitham's theory.

Shock Wave Location Method

Concurrently with steps 2 through 5 above, a method would be developed to estimate the location of the shock waves in the field, based on the first-order velocity components and pressure signature. The principle that the slope of the shock wave lies halfway between the slopes of the first-order Mach waves directly ahead and behind it would be applied to determine shock wave location. Much emphasis would be placed on the method developed by Whitham for locating shock waves, and an attempt would be made to determine if the equal-area technique would still be applicable to this problem. In particular, the problem of determining the distance from a body at which multiple shocks coalesce would be studied.

26

CONCLUSIONS

The feasibility of extending the existing supersonic wing-body analysis program (reference 1) to the calculation of the pressure signature, including shock waves, of an arbitrary wing-body or airplane configuration has been investigated. The conclusion reached is that theoretical methods are presently available to make this extension possible, and a program to develop these methods in an orderly fashion has been outlined in some detail.

The method presented in this report could serve as a useful adjunct to Whitham's theory for calculating the pressure signatures and shock wave locations and strengths in both the near and far fields surrounding arbitrary airplane configurations. In particular, it has the advantage of allowing the calculation of the surface pressures, forces, and moments acting on the configuration while giving a uniformly valid first-order solution in the entire flow field. No slender-body and slender-wing theory assumptions are required in the singularity representation, so that the effects of the spatial distribution of the singularities is fully accounted for at all distances from the body. This feature of the new method could result in improved estimates of shock wave coalesence in the near field and corresponding improvements in the prediction of the location and magnitude of the intermediate shock jumps for pressure signatures not fully developed into the asymptotic N wave form.

The design implications of the method are important. Since the pressure signature is made up of summations of integrals of elementary velocity components and depends linearly on the strengths of the singularities used to represent the configuration, a linear system of equations can be derived relating the pressure signature properties to configuration geometry. It may then be possible to formulate several interesting optimization problems relating the shape and intensity of the pressure signature to the airplane volume, lift, drag, and moment.

All the theory presented in this study has been made assuming a uniform atmosphere. The effects of nonuniformity in the atmosphere would necessarily involve corrections of the type outlined in references 4 and 5.

The Boeing Company
  Commercial Airplane Division
    Renton, Washington
      August 15, 1967
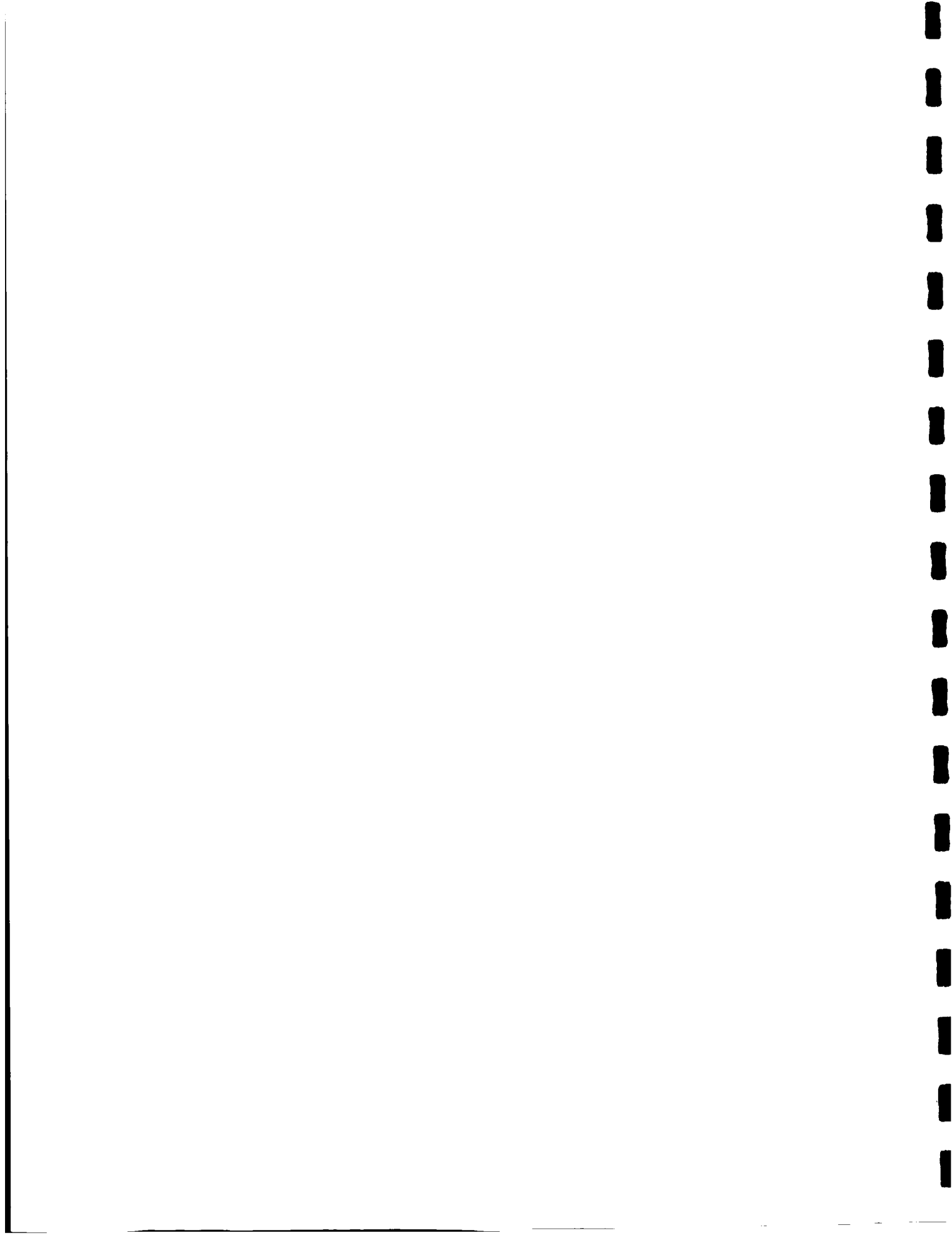
Tabulation of Velocity Components

Line Singularities

1. Linear Source

$$u = -k_1 \cosh^{-1} t$$

$$v_r = \beta k_1 \sqrt{t^2 - 1}$$

$$v_\theta = 0$$

2. Quadratic Source

$$u = -2k_2 x \left(\cosh^{-1} t - \frac{1}{t}\sqrt{t^2 - 1} \right)$$

$$v_r = \beta k_2 x \left(\sqrt{t^2 - 1} - \frac{1}{t} \cosh^{-1} t \right)$$

$$v_\theta = 0$$

3. Linear Doublet

$$u = \beta k_3 \cos\theta \sqrt{t^2 - 1}$$

$$v_r = -\frac{\beta k_3 \cos\theta}{2} \left(\cosh^{-1} t + t\sqrt{t^2 - 1} \right)$$

$$v_\theta = \frac{\beta^2 k_3 r \sin\theta}{2} \left(\cosh^{-1} t - t\sqrt{t^2 - 1} \right)$$

4. Quadratic Doublet

$$u = \beta k_4 x \cos\theta \left(\sqrt{t^2 - 1} - \frac{1}{t} \cosh^{-1} t \right)$$

$$v_r = -\beta^2 k_4 x \cos\theta \left(\cosh^{-1} t + \frac{1}{3}\left(t - \frac{4}{t}\right)\sqrt{t^2 - 1} \right)$$

$$v_\theta = \beta^2 k_4 x r \sin\theta \left(\cosh^{-1} t - \frac{1}{3}\left(t + \frac{2}{t}\right)\sqrt{t^2 - 1} \right)$$

Planar Singularities

1. Constant Source Sheet

$$u = -\frac{\overline{w}}{\pi} \frac{m}{\sqrt{1 - \beta^2 m^2}} \cosh^{-1} \frac{t - \beta m \cos\theta}{\sqrt{(\beta m t - \cos\theta)^2 + (1 - \beta^2 m^2)\sin^2\theta}}$$

$$v = \frac{\overline{w}}{\pi} \left(\frac{1}{\sqrt{1 - \beta^2 m^2}} \cosh^{-1} \frac{t - \beta m \cos\theta}{\sqrt{(\beta m t - \cos\theta)^2 + (1 - \beta^2 m^2)\sin^2\theta}} - \cosh^{-1} t \right)$$

$$w = \frac{\overline{w}}{\pi} \tan^{-1} \frac{m \sin\theta \sqrt{t^2 - 1}}{1 - \beta m t \cos\theta}$$

2. Linear Source Sheet

$$u = \frac{\overline{w}_x}{\pi} mr \left(\frac{\beta mt - \cos\theta}{\sqrt{1 - \beta^2 m^2}} \cosh^{-1} \frac{t - \beta m \cos\theta}{\sqrt{(\beta mt - \cos\theta)^2 + (1 - \beta^2 m^2)\sin^2\theta}} \right.$$

$$\left. + \cos\theta \cosh^{-1} t - \sin\theta \tan^{-1} \frac{m\sin\theta\sqrt{t^2 - 1}}{1 - \beta m t \cos\theta} \right)$$

$$v = \frac{\overline{w}_x}{\pi} r \left[(\beta mt - \cos\theta) \cdot \right.$$

$$\left(\cosh^{-1} t - \frac{1}{\sqrt{1 - \beta^2 m^2}} \cosh^{-1} \frac{t - \beta m \cos\theta}{\sqrt{(\beta mt - \cos\theta)^2 + (1 - \beta^2 m^2)\sin^2\theta}} \right)$$

$$\left. + \sin\theta \tan^{-1} \frac{m\sin\theta\sqrt{t^2 - 1}}{1 - \beta mt \cos\theta} - m\sqrt{t^2 - 1} \right]$$

$$w = \frac{\overline{w}_x}{\pi} r \left[\sin\theta \cdot \right.$$

$$\left(\cosh^{-1} t - \sqrt{1 - \beta^2 m^2} \cosh^{-1} \frac{t - \beta m \cos\theta}{\sqrt{(\beta mt - \cos\theta)^2 + (1 - \beta^2 m^2)\sin^2\theta}} \right)$$

$$\left. - (\beta mt - \cos\theta) \tan^{-1} \frac{m\sin\theta\sqrt{t^2 - 1}}{1 - \beta mt \cos\theta} \right]$$

3. Constant Vortex Sheet

$$u = \frac{\overline{u}}{\pi} \tan^{-1} \frac{m\sin\theta\sqrt{t^2 - 1}}{1 - \beta mt \cos\theta}$$

$$v = -\frac{\overline{u}}{\pi} \left(\tan^{-1} \frac{m\sin\theta\sqrt{t^2 - 1}}{1 - \beta mt \cos\theta} - m\sin\theta\sqrt{t^2 - 1} \right)$$

$$w = \frac{\overline{u}}{\pi m} \left(\sqrt{1 - \beta^2 m^2} \cosh^{-1} \frac{t - \beta m \cos\theta}{\sqrt{(\beta mt - \cos\theta)^2 + (1 - \beta^2 m^2)\sin^2\theta}} \right.$$

$$\left. - \cosh^{-1} t - m\cos\theta\sqrt{t^2 - 1} \right)$$

where

$$t = \frac{x}{\beta r}$$

and

$$m = \cot \Lambda$$

Note: $\beta \equiv \beta_\infty$ in this appendix.

30

The above formulas are written for the subsonic leading edge case $m < \beta$. For the supersonic leading edge case, replace the function

$$\frac{1}{\sqrt{1 - \beta^2 m^2}} \cosh^{-1} \frac{t - \beta m \cos\theta}{\sqrt{(\beta m t - \cos\theta)^2 + (1 - \beta^2 m^2) \sin^2\theta}}$$

by

$$\frac{1}{\sqrt{\beta^2 m^2 - 1}} \cos^{-1} \frac{t - \beta m \cos\theta}{\sqrt{(\beta m t - \cos\theta)^2 + (1 - \beta^2 m^2) \sin^2\theta}}$$

APPENDIX II

Tabulation of Integrals

$$I_1 = \int \cosh^{-1} (1 + t_0) \, dr$$

$$= r \left[\cosh^{-1} (1 + t_0) + \sqrt{t_0 (2 + t_0)} \right] \tag{A1}$$

$$I_2 = \int \sqrt{t_0 (2 + t_0)} \, dr$$

$$= \frac{x_0}{\beta} \left[2\sqrt{1 + \frac{2}{t_0}} - \cosh^{-1} (1 + t_0) \right] \tag{A2}$$

$$I_3 = \int \cosh^{-1} \frac{1 + t_0 - \beta m \cos \theta}{\sqrt{\left(\beta m(1 + t_0) - \cos \theta\right)^2 + \left(1 - \beta^2 m^2\right) \sin^2 \theta}} \, dr$$

$$= \frac{x_0}{\beta} \left\{ \left[\frac{1}{t_0} + \frac{\beta m(\beta m - \cos \theta)}{(1 - \beta m \cos \theta)^2} \right] \cosh^{-1} \frac{1 + t_0 - \beta m \cos \theta}{\sqrt{\left(\beta m(1 + t_0) - \cos \theta\right)^2 + (1 - \beta^2 m^2) \sin^2 \theta}} \right.$$

$$+ \frac{\sqrt{1 - \beta^2 m^2}}{1 - \beta m \cos \theta} \sqrt{1 + \frac{2}{t_0}}$$

$$\left. + \frac{\beta m \cos \theta \sqrt{1 - \beta^2 m^2}}{(1 - \beta m \cos \theta)^2} \tan^{-1} \frac{\beta m t_0 \sin \theta \sqrt{1 + \frac{2}{t_0}}}{1 - \beta m \cos \theta (1 + t_0)} \right\} \tag{A3}$$

$$I_4 = \int \tan^{-1} \frac{\beta m t_0 \sin \theta \sqrt{1 + \frac{2}{t_0}}}{1 - \beta m \cos \theta (1 + t_0)} \, dr$$

$$= \frac{x_0}{\beta} \left\{ \left[\frac{1}{t_0} + \frac{\beta m(\beta m - \cos \theta)}{(1 - \beta m \cos \theta)^2} \right] \tan^{-1} \frac{\beta m t_0 \sin \theta \sqrt{1 + \frac{2}{t_0}}}{1 - \beta m \cos \theta (1 + t_0)} \right.$$

$$+ \frac{\beta m \sin \theta}{1 - \beta m \cos \theta} \sqrt{1 + \frac{2}{t_0}}$$

$$\left. - \frac{\beta m \sin \theta \sqrt{1 - \beta^2 m^2}}{(1 - \beta m \cos \theta)^2} \cosh^{-1} \frac{1 + t_0 - \beta m \cos \theta}{\sqrt{\left(\beta m(1 + t_0) - \cos \theta\right)^2 + (1 - \beta^2 m^2) \sin^2 \theta}} \right\} \tag{A4}$$

$$I_5 = \int r \cosh^{-1}(1 + t_0)\, dr$$

$$= \frac{r^2}{2}\left[\cosh^{-1}(1 + t_0) + \frac{1}{3}(1 - t_0)\sqrt{t_0(2 + t_0)}\right] \tag{A5}$$

$$I_6 = \int r\sqrt{t_0(2 + t_0)}\, dr$$

$$= \frac{x_0^2}{3\beta^2}\left(1 + \frac{2}{t_0}\right)^{3/2} \tag{A6}$$

$$I_7 = \int \frac{\sqrt{t_0(2 + t_0)}}{r}\, dr$$

$$= -t_0\sqrt{1 + \frac{2}{t_0}} - \cosh^{-1}(1 + t_0) \tag{A7}$$

$$I_8 = \frac{x_0}{\beta}\int r \cosh^{-1}\frac{1 + t_0 - \beta m \cos\theta}{\sqrt{(\beta m(1 + t_0) - \cos\theta)^2 + (1 - \beta^2 m^2)\sin^2\theta}}\, dr$$

$$= \frac{x_0}{\beta}\left\{\frac{r^2}{2}\cosh^{-1}\frac{1 + t_0 - \beta m \cos\theta}{\sqrt{(\beta m(1 + t_0) - \cos\theta)^2 + (1 - \beta^2 m^2)\sin^2\theta}}\right.$$

$$+ \frac{x_0^2\sqrt{1 - \beta^2 m^2}}{4(1 - \beta m \cos\theta)}\sqrt{1 + \frac{2}{t_0}}\left[\frac{1}{3}\left(1 + \frac{2}{t_0}\right) - \frac{1 - \beta^2 m^2\cos^2\theta + 4\beta m(\beta m - \cos\theta)}{\beta(1 - \beta m \cos\theta)^2}\right]$$

$$- \frac{m^2 x_0^2}{(1 - \beta m \cos\theta)^4}\left[\frac{(\beta m - \cos\theta)^2 - (1 - \beta^2 m^2)\sin^2\theta}{2}\right.\cdot$$

$$\cosh^{-1}\frac{1 + t_0 - \beta m \cos\theta}{\sqrt{(\beta m(1 + t_0) - \cos\theta)^2 + (1 - \beta^2 m^2)\sin^2\theta}}$$

$$\left.\left. + \sin\theta\,(\beta m - \cos\theta)\sqrt{1 - \beta^2 m^2}\,\tan^{-1}\frac{\beta m t_0 \sin\theta\sqrt{1 + \frac{2}{t_0}}}{1 - \beta m \cos\theta\,(1 + t_0)}\right]\right\} \tag{A8}$$

$$I_9 = \frac{x_0}{\beta} \int r \tan^{-1} \frac{\beta m t_0 \, \sin\theta \, \sqrt{1 + \dfrac{2}{t_0}}}{1 - \beta m \, \cos\theta \, (1 + t_0)} \, dr$$

$$= \frac{x_0}{\beta} \left\{ \frac{r^2}{2} \tan^{-1} \frac{\beta m t_0 \, \sin\theta \, \sqrt{1 + \dfrac{2}{t_0}}}{1 - \beta m \, \cos\theta \, (1 + t_0)} \right.$$

$$+ \frac{m^2 x_0^{\,2} \, \sin\theta}{4(1 - \beta m \, \cos\theta)} \sqrt{1 + \frac{2}{t_0}} \left[\frac{1}{3} \left(1 + \frac{2}{t_0} \right) \right.$$

$$+ \left. \frac{\sin\theta \left(1 - \beta^2 m^2 \cos^2\theta - 4\beta m (\beta m - \cos\theta) \right)}{(1 - \beta m \, \cos\theta)^2} \right]$$

$$+ \frac{\beta m^3 x_0^{\,2} \, \sin\theta}{(1 - \beta m \, \cos\theta)^4} \left[\sin\theta \, (\beta m - \cos\theta) \sqrt{1 - \beta^2 m^2} \; \cdot \right.$$

$$\cosh^{-1} \frac{1 + t_0 - \beta m \, \cos\theta}{\sqrt{(\beta m (1 + t_0) - \cos\theta)^2 + (1 - \beta^2 m^2) \, \sin^2\theta}}$$

$$- \left. \left. \frac{(\beta m - \cos\theta)^2 - (1 - \beta^2 m^2) \, \sin^2\theta}{2} \tan^{-1} \frac{\beta m t_0 \, \sin\theta \, \sqrt{1 + \dfrac{2}{t_0}}}{1 - \beta m \, \cos\theta \, (1 + t_0)} \right] \right\} \tag{A9}$$

where

$$t_0 = \frac{x_0}{\beta r}$$

and

$$\beta \equiv \beta_\infty$$

REFERENCES

1. Woodward, F. A.; Tinoco, E.N.; and Larsen, J.W.: Analysis and Design of Supersonic Wing-Body Combinations, Including Flow Properties in the Near Field, Part I — Theory and Application. NASA CR-73106, August 1967.

2. Whitham, G.B.: The Flow Pattern of a Supersonic Projectile. Communications on Pure and Applied Mathematics, vol. V, 1952, pp. 301-348.

3. Lighthill, M.J.: The Shock Strengths in Supersonic Conical Fields. Philosophical Magazine vol. 40, 1949, p. 1202.

4. Friedman, M.P.; Kane, E.J.; and Sigalla, A.: Effects of Atmosphere and Aircraft Motion on the Location and Intensity of a Sonic Boom. AIAA Journal, vol. 1, no. 6, June 1963.

5. Kane, E.J.: Some Effects of the Nonuniform Atmosphere on the Propagation of Sonic Booms. J. Acoust. Soc. Am., vol. 39, no. 5, pt. 2, May 1966.